

# Efficient 3D-Finite-Element-Formulation for Thin Mechanical and Piezoelectric Structures

Dietrich Braess<sup>1</sup>, Manfred Kaltenbacher<sup>2\*</sup>

<sup>1</sup>*Faculty of Mathematics, Ruhr-University, Bochum, Germany*

<sup>2</sup>*Department of Sensor Technology, Friedrich-Alexander University Erlangen-Nuremberg, Germany*

## SUMMARY

It is the aim to compute efficiently the deformations of the mechanical structures that are excited or damped by piezoelectric actuators. They are treated as 3D structures to have much flexibility. Special design of the finite element concept is required since the structures are thin walled and locking effects have to be avoided. Although the computations are performed in the framework of 3-dimensional elasticity, we use ideas from modern plate elements and mixed methods.

Copyright © 2000 John Wiley & Sons, Ltd.

KEY WORDS: structural mechanics, piezoelectrics, mixed finite elements, displacement based formulation, shear locking

## 1. Introduction

The piezoelectric effect is used in many modern mechatronic sensors, actuators as well as sensor-actuator-systems. We will focus here on the use of the piezoelectric effect to generate sound (e.g. piezoelectric loudspeaker) or to compensate mechanical vibrations by distributed piezoelectric patches on thin walled bodies. Usually these bodies consists of mechanical parts like plates or shells with a small curvature. It is the aim to efficiently compute the deformations of the mechanical structures that are excited or damped by piezoelectric actuators.

In order to have enough flexibility we treat the mechanical as well as piezoelectric structure as a 3-dimensional body in the framework of 3-dimensional elasticity. It is well known, that finite element calculations require special design in order to exclude locking effects (as e.g. shear locking), since the thickness is here a small parameter and we want to avoid finite elements with polynomials of higher degree. The remedy is an appropriate softening of the shear term of the stored energy. This can be done in the framework of the method of enhanced assumed strains (EAS-method) or by selected reduced integration when the element stiffness matrix is assembled. Our procedure will be motivated by recent developments for the Mindlin–Reissner

---

\*Correspondence to: Department of Sensor Technology Friedrich-Alexander University Erlangen-Nuremberg, Paul-Gordan-Str. 3-5, D-91052 Erlangen, Germany  
e-mail: manfred@lse.eei.uni-erlangen.de

plate by Arnold and Brezzi [1] as well as Chapelle and Stenberg [5]; see also [4]. We apply selected reduced integration only to a portion of the shear term. The amount of the portion is derived by a scaling argument. In this way we obtain a robust finite element treatment and do not encounter zero-energy modes or checkerboard modes while caring for the elimination of locking.

The rest of this paper is organized as follows. In Sec. 2 we describe the governing equations for piezoelectricity and discuss their finite element (FE) formulation. The theory of our new procedure to obtain an approximate softening of the shear term is presented in Sec. 3. It is followed by a brief section describing some practical aspects for the computer implementation. Section 5 provides a detailed discussion of numerical results, where we compare our method with the Mindlin–Reissner plate bending element of Hughes and Tezduyar [7] and the Mindlin–Reissner plate bending element of Simo and Rifai based on the method of enhanced assumed strains (EAS method) [11]. In addition, we investigate the dynamic behavior of mechanical structures and layered mechanical-piezoelectric structures. To demonstrate the capability of our method for piezoelectric structures we present in Sec. 5.6 the numerical computations for a piezoelectric loudspeaker.

## 2. Governing PDEs and FE-Formulation

The piezoelectric transducing mechanism is based on the interaction between the electric quantities, electric field intensity  $\mathbf{E}$  and electric induction  $\mathbf{D}$ , with the mechanical quantities, i.e., the (mechanical) stress tensor  $[\boldsymbol{\sigma}]$  and strain tensor  $[\mathbf{S}]^\dagger$ . By applying a mechanical load (force) to a piezoelectric transducer (e.g., piezoelectric material with top and bottom electrode), one can measure an electric voltage between the two electrodes (sensor effect). This mechanism is called the *direct piezoelectric effect*, and is due to a change in the electric polarization of the material. The so-called *inverse piezoelectric effect* is obtained by loading a piezoelectric transducer with an electric voltage. Therewith, the transducer will show mechanical deformations (actuator effect), and the setup can be used, e.g., in a positioning system.

The material law describing the piezoelectric effect is given by

$$\boldsymbol{\sigma} = [\mathbf{c}^E] \mathbf{S} - [\mathbf{e}]^T \mathbf{E}, \quad (1)$$

$$\mathbf{D} = [\mathbf{e}] \mathbf{S} + [\boldsymbol{\epsilon}^S] \mathbf{E}. \quad (2)$$

Since the stress tensor  $[\boldsymbol{\sigma}]$  as well as the strain tensor  $[\mathbf{S}]$  are symmetric, it is convenient to write them as vectors of six components (the three normal and the three shear components) using *Voigt notation* and denote them by  $\boldsymbol{\sigma}$  and  $\mathbf{S}$  [3]. The material tensors  $[\mathbf{c}^E]$ ,  $[\boldsymbol{\epsilon}^S]$ , and  $[\mathbf{e}]$  appearing in (1) and (2) are the tensor of elastic modulus, of dielectric constants, and of piezoelectric moduli, respectively. The superscripts  $E$  and  $S$  indicate that the corresponding material parameters have to be determined at constant electric field intensity  $\mathbf{E}$  and at constant mechanical strain  $\mathbf{S}$ , respectively.

---

<sup>†</sup>We denote the mechanical strain tensor by  $\mathbf{S}$ , since  $\boldsymbol{\epsilon}$  is reserved for the electric permittivity within the context of piezoelectricity

For deriving the coupled PDEs for piezoelectricity, we start at Navier's equation

$$\mathbf{f}_V + \mathbf{div} \boldsymbol{\sigma} = \rho \ddot{\mathbf{u}}, \quad (3)$$

describing the mechanical field. In (3)  $\mathbf{f}_V$  denotes any mechanical volume force,  $\rho$  the density and  $\mathbf{u}$  the mechanical displacement. Expressing  $\boldsymbol{\sigma}$  by (1) and in-cooperating the strain-displacement relation

$$\mathbf{S} = \nabla^s \mathbf{u} = \mathcal{B} \mathbf{u} \quad (4)$$

with the differential operator  $\mathcal{B}$  in Voigt notation

$$\mathcal{B} = \begin{pmatrix} \frac{\partial}{\partial x} & 0 & 0 & 0 & \frac{\partial}{\partial z} & \frac{\partial}{\partial y} \\ 0 & \frac{\partial}{\partial y} & 0 & \frac{\partial}{\partial z} & 0 & \frac{\partial}{\partial x} \\ 0 & 0 & \frac{\partial}{\partial z} & \frac{\partial}{\partial y} & \frac{\partial}{\partial x} & 0 \end{pmatrix}^T, \quad (5)$$

results in

$$\rho \ddot{\mathbf{u}} - \mathcal{B}^T ([\mathbf{c}^E] \mathcal{B} \mathbf{u} - [\mathbf{e}]^T \mathbf{E}) = \mathbf{f}_V. \quad (6)$$

Since piezoelectric materials are insulating, i.e., they do not contain free-volume charges, and we do not have to consider any magnetic field, the electric field is determined by

$$\nabla \cdot \mathbf{D} = 0, \quad (7)$$

$$\nabla \times \mathbf{E} = 0. \quad (8)$$

According to (8) we can express the electric field intensity  $\mathbf{E}$  by the gradient of the scalar electric potential  $V_e$

$$\mathbf{E} = -\nabla V_e = -\tilde{\mathcal{B}} V_e \quad \tilde{\mathcal{B}} = (\partial/\partial x, \partial/\partial y, \partial/\partial z)^T. \quad (9)$$

By combining these results with (2) we obtain

$$\mathcal{B}^T ([\mathbf{e}] \mathcal{B} \mathbf{u} - [\boldsymbol{\varepsilon}^S] \tilde{\mathcal{B}} V_e) = q_e. \quad (10)$$

Therefore, the describing partial differential equations for linear piezoelectricity read as

$$\rho \ddot{\mathbf{u}} - \mathcal{B}^T ([\mathbf{c}^E] \mathcal{B} \mathbf{u} + [\mathbf{e}]^T \tilde{\mathcal{B}} V_e) = \mathbf{f}_V \quad (11)$$

$$\mathcal{B}^T ([\mathbf{e}] \mathcal{B} \mathbf{u} - [\boldsymbol{\varepsilon}^S] \tilde{\mathcal{B}} V_e) = 0. \quad (12)$$

By applying a standard FE-formulation, we obtain the following semi-discrete Galerkin formulation

$$\begin{pmatrix} \mathbf{M}_u & 0 \\ 0 & 0 \end{pmatrix} \begin{pmatrix} \ddot{\underline{u}} \\ \ddot{\underline{V}}_e \end{pmatrix} + \begin{pmatrix} \mathbf{C}_u & 0 \\ 0 & 0 \end{pmatrix} \begin{pmatrix} \dot{\underline{u}} \\ \dot{\underline{V}}_e \end{pmatrix} + \begin{pmatrix} \mathbf{K}_u & \mathbf{K}_{uV} \\ \mathbf{K}_{uV}^T & -\mathbf{K}_V \end{pmatrix} \begin{pmatrix} \underline{u} \\ \underline{V}_e \end{pmatrix} = \begin{pmatrix} 0 \\ \underline{f}_q \end{pmatrix}. \quad (13)$$

In (13), the matrices  $\mathbf{M}_u$  and  $\mathbf{K}_u$  denote the mechanical mass and stiffness matrix,  $\mathbf{K}_V$  the electrostatic stiffness matrix,  $\mathbf{K}_{uV}$  the coupling matrix, and  $\underline{f}_q$  the mechanical force vector. The mechanical damping matrix  $\mathbf{C}_u$  is computed according to the Rayleigh damping model via a combination of the mass matrix  $\mathbf{M}_u$  and the linear stiffness matrix  $\mathbf{K}_u$

$$\mathbf{C}_u = \alpha_M \mathbf{M}_u + \alpha_K \mathbf{K}_u \quad (14)$$

with  $\alpha_M$  the mass proportional and  $\alpha_K$  the stiffness proportional damping coefficients [6]. For the time discretization, Newmark's algorithm as described in [6] is used. In the frequency domain we obtain according to (13)

$$\begin{pmatrix} \mathbf{K}_u + j\omega\mathbf{C}_u - \omega^2\mathbf{M}_u & \mathbf{K}_{uV} \\ \mathbf{K}_{uV}^T & -\mathbf{K}_V \end{pmatrix} \begin{pmatrix} \hat{\underline{u}} \\ \hat{\underline{V}}_e \end{pmatrix} = \begin{pmatrix} 0 \\ \hat{\underline{f}}_q \end{pmatrix} \quad (15)$$

with  $\omega = 2\pi f$  the angular frequency. For a detailed discussion we refer to [8].

### 3. Theoretical Aspects

The deformation of the body on which the piezoelectric material is mounted, will be computed in the framework of 3-dimensional elasticity. We consider a 3-dimensional body with thickness  $2t$ . Since  $t$  is small in applications of interest, we take special care for avoiding locking effects. To this end we will compare the trial functions later with those of a well-established Mindlin–Reissner plate model and justify the procedure.

The finite element functions with quadratic polynomials in  $z$  are written with orthogonal polynomials in  $z$

$$u_i(x, y, z) = U_i(x, y) + z\theta_i(x, y) + \left(z^2 - \frac{t^2}{3}\right)\phi_i(x, y), \quad i = 1, 2, 3. \quad (16)$$

For convenience, we also write  $x_1 = x$ ,  $x_2 = y$  and  $x_3 = z$  when evaluating the strains  $S_{ik} = \frac{1}{2}\left(\frac{\partial u_i}{\partial x_k} + \frac{\partial u_k}{\partial x_i}\right)$ . In particular,

$$S_{i3} = \frac{1}{2}\left(\theta_i + \frac{\partial U_3}{\partial x_i}\right) + \frac{1}{2}z\left(2\phi_i + \frac{\partial\theta_3}{\partial x_i}\right) + \frac{1}{2}\left(z^2 - \frac{t^2}{3}\right)\left(\frac{\partial\phi_3}{\partial x_i}\right), \quad i = 1, 2. \quad (17)$$

By integrating over the thickness we obtain

$$\begin{aligned} \int S_{ii}^2 dz &= 2t\left(\frac{\partial U_i}{\partial x_i}\right)^2 + \underbrace{\frac{2}{3}t^3\left(\frac{\partial\theta_i}{\partial x_i}\right)^2 + \frac{8}{45}t^5\left(\frac{\partial\phi_i}{\partial x_i}\right)^2}_{\text{MR-plate}}, \quad i = 1, 2, \\ \int S_{12}^2 dz &= \frac{1}{2}t\left(\frac{\partial U_1}{\partial x_2} + \frac{\partial U_2}{\partial x_1}\right)^2 + \underbrace{\frac{1}{6}t^3\left(\frac{\partial\theta_1}{\partial x_2} + \frac{\partial\theta_2}{\partial x_1}\right)^2 + \frac{2}{45}t^5\left(\frac{\partial\phi_1}{\partial x_2} + \frac{\partial\phi_2}{\partial x_1}\right)^2}_{\text{MR-plate}}, \\ \int S_{33}^2 dz &= 2t\theta_3^2 + \frac{8}{3}t^3\phi_3^2, \\ \int S_{i3}^2 dz &= \underbrace{\frac{1}{2}t\left(\theta_i + \frac{\partial U_3}{\partial x_i}\right)^2}_{\text{MR-plate}} + \frac{1}{6}t^3\left(2\phi_i + \frac{\partial\theta_3}{\partial x_i}\right)^2 + \frac{2}{45}t^5\left(\frac{\partial\phi_3}{\partial x_i}\right)^2, \quad i = 1, 2. \end{aligned}$$

The terms that are encountered in Mindlin–Reissner plate theory are emphasized by the mark 'MR-plate'.

The internal stored energy of the solution is proportional to  $t^3$ . We avoid locking if the terms with a factor proportional to  $t$  do not spoil the finite element solution. The terms with  $U_1$

and  $U_2$  are easily analyzed. It follows from Korn's inequality that the gradients of  $U_1$  and  $U_2$  contribute to the energy if they are not small. Therefore,  $U_1$  and  $U_2$  must be small of order  $t$ , since the contribution to the internal stored energy is of order  $t^3$ . Obviously the same holds for  $\theta_3$ . This is consistent with the fact that these terms are set to zero in plate theory.

The critical terms are the shear terms with  $S_{i3}$ . The terms  $\theta_i$  and  $\partial U_3/\partial x_i$  are not small while the sum is small of order  $t$ . This property cannot be modeled by standard finite elements with polynomials of low degree, and the first term in the integral with  $S_{i3}$  is relaxed in finite element computations. It is our aim to avoid a rude softening by referring to recent treatment of Mindlin-Reissner plates.

We first consider the case that only polynomials are chosen that are linear in  $z$ , i.e., we have

$$\phi_i = 0, \quad i = 1, 2, 3,$$

in (16). In this case the shear term is softened as follows. The full integral is incorporated with a factor

$$\alpha = \frac{t^2}{h^2 + t^2} \quad (18)$$

while selected reduced integration is applied to the rest of the shear term, i.e., to the portion

$$\beta = 1 - \alpha = \frac{h^2}{h^2 + t^2}. \quad (19)$$

Specifically, quadrature formulas with 1 point in the  $x, y$ -plane are used. This procedure is equivalent (on parallelograms) to incorporating only the integral of the squared mean-value of  $\theta_i + \partial U_3/\partial x_i$  on each element. The idea to apply a softening only to a portion of the shear term in order to save coercivity was first suggested by [1]. The factors  $\alpha$  and  $\beta$  in (18) and (19) are fixed following the results in [5]. The shear term is a singular perturbation in comparison to the other terms of the internal stored energy. The importance of keeping the coercivity and not reducing the full term was discussed in [4, Section 6.6] in the framework of saddle point problems with penalty terms. So our approach differs from the typical application of the EAS concept; see e.g. [10].

The correct softening is more involved if *quadratic polynomials* in  $z$  are present. Only the first term in  $\int S_{i3}^2$  is to be reduced, but the second term must not. This can be realized by different implementations.

The most direct way is to keep the three terms in  $\int S_{i3}^2$  separated during the assembling of the stiffness matrix and the whole finite element computation. So it is possible to apply the selected reduced integration only to the critical term, i.e., the first one.

An alternative is a separation of the even and the odd functions in  $z$ , and it goes with  $\phi_3 = 0$ . Recalling (17) we see that a softening of the even part of  $S_{i3}$  is required. Note that

$$\begin{aligned} \int_{-t}^{+t} S_{i3}^2(x, y, z) dz &= \frac{1}{2} \int_{-t}^{+t} (S_{i3}(x, y, z) + S_{i3}(x, y, -z))^2 dz \\ &+ \frac{1}{2} \int_{-t}^{+t} (S_{i3}(x, y, z) - S_{i3}(x, y, -z))^2 dz. \end{aligned} \quad (20)$$

A separation of the first and the second term is performed here via a symmetry argument. Only a portion of the even part (with the weight  $\beta$ ) is incorporated into the selected reduced integration. This method will be applied to our computational scheme as described in Section 4.

A third possibility provides the EAS method (more precisely *selected* EAS method). We replace the standard trial functions for  $S_{i3}$  by

$$S_{i3} + \hat{S}_{i3}$$

with the enhanced strain being in each element of the form  $\hat{S}_{i3} = a(x - x_c) + b(y - y_c)$ , where  $x_c$  and  $y_c$  are the (local) coordinates of the center of the element. The mean value of the enhanced strain in each element is zero, and yields an appropriate softening. Since it does not depend on  $z$ , it acts only on the even part of the shear term. – Although one finds in the literature investigations with the EAS method applied to the complete shear term, the extension to a portion with a given factor is straight forward.

Now we can justify the numerical procedure by referring to arguments concerning dimension reduction, but here in the opposite direction. As was shown in [9,12] and the references therein, the plate models are exact of order  $t$  or  $t^{1/2}$ . (The latter occurs if boundary layers are present.) Since the finite element functions (16) contain more trial functions than the plate models [1,5], our finite element solutions in 3D produce even smaller errors. In particular, locking effects are avoided by a procedure which requires less softening than is found in most EAS applications.

Fortunately there are no point loads in mechatronic systems with piezoelectric actuators. Otherwise we would have to compare with MITC elements (see e.g. [4, p. 328]) or nonconforming elements in [2] as was pointed out in [9].

#### 4. Practical Aspects of the Computer Implementation

As described in the previous section, the shear components are proportional to the thickness  $t$  of the structure, whereas the bending terms scale with  $t^3$ . We decompose the material tensor  $[\mathbf{c}^E]$  with the scaling from (18) and (19) as follows.

$$[\mathbf{c}^E] = [\mathbf{c}^E]_\alpha + [\mathbf{c}^E]_\beta \quad (21)$$

$$[\mathbf{c}^E]_\alpha = \begin{pmatrix} c_{11} & c_{12} & c_{13} & 0 & 0 & 0 \\ c_{21} & c_{22} & c_{23} & 0 & 0 & 0 \\ c_{31} & c_{32} & c_{33} & 0 & 0 & 0 \\ 0 & 0 & 0 & \alpha c_{44} & 0 & 0 \\ 0 & 0 & 0 & 0 & \alpha c_{44} & 0 \\ 0 & 0 & 0 & 0 & 0 & c_{66} \end{pmatrix}, \quad \alpha = \frac{t^2}{h^2 + t^2}, \quad (22)$$

$$[\mathbf{c}^E]_\beta = \begin{pmatrix} 0 & 0 & 0 & 0 & 0 & 0 \\ 0 & 0 & 0 & 0 & 0 & 0 \\ 0 & 0 & 0 & 0 & 0 & 0 \\ 0 & 0 & 0 & \beta c_{44} & 0 & 0 \\ 0 & 0 & 0 & 0 & \beta c_{44} & 0 \\ 0 & 0 & 0 & 0 & 0 & 0 \end{pmatrix}, \quad \beta = \frac{h^2}{h^2 + t^2}. \quad (23)$$

In (22) and (23)  $h$  denotes the largest side length and  $t$  the smallest side length (for thin structures  $t$  corresponds to the thickness) of the elements. Therewith, the element stiffness

matrix  $\mathbf{k}_u^e$  of the mechanical part computes as

$$\begin{aligned}
\mathbf{k}_u^e &= \sum_{i=1}^{14} \mathcal{B}_i^T [\mathbf{c}^E]_\alpha \mathcal{B} |\mathcal{J}_i| w_i^{\text{std}} \\
&+ \frac{1}{2} \sum_{i=5}^9 (\mathcal{B}_{i+5} - \mathcal{B}_i)^T [\mathbf{c}^E]_\beta (\mathcal{B}_{i+5} - \mathcal{B}_i) |\mathcal{J}_i| w_i^{\text{std}} \\
&+ \frac{1}{2} (\mathcal{B}_3 + \mathcal{B}_1)^T [\mathbf{c}^E]_\beta (\mathcal{B}_3 + \mathcal{B}_1) |\mathcal{J}_1| w_1^{\text{red}} \\
&+ \mathcal{B}_2^T [\mathbf{c}^E]_\beta \mathcal{B}_2 |\mathcal{J}_2| w_2^{\text{red}}
\end{aligned} \tag{24}$$

where  $|\mathcal{J}_i|$  denotes the Jacobian determinant at integration point  $i$ . As can be seen from (24), the first two terms are integrated by the standard scheme (see Tab. I) and the last two terms by the reduced scheme (see Tab. II). In particular, only the symmetrical part of the critical shear term is dealt with by reduced integration, and the decomposition (20) is used for this purpose.

Table I. Points and weights for the standard integration

$\xi_i$	$\eta_i$	$\zeta_i$	$w_i^{\text{std}}$
0.7958	0.0	0.0	0.8864
-0.7958	0.0	0.0	0.8864
0.0	0.7958	0.0	0.8864
0.0	-0.7958	0.0	0.8864
0.0	0.0	-0.7958	0.8864
0.7588	0.7588	-0.7588	0.3352
0.7588	-0.7588	-0.7588	0.3352
-0.7588	0.7588	-0.7588	0.3352
-0.7588	-0.7588	-0.7588	0.3352
0.0	0.0	0.7958	0.8864
0.7588	0.7588	0.7588	0.3352
0.7588	-0.7588	0.7588	0.3352
-0.7588	0.7588	0.7588	0.3352
-0.7588	-0.7588	0.7588	0.3352

Table II. Points and weights for the reduced integration

$\xi_i$	$\eta_i$	$\zeta_i$	$w_i^{\text{red}}$
0	0	$-1/\sqrt{3}$	8/3
0	0	0	8/3
0	0	$1/\sqrt{3}$	8/3

## 5. Numerical Case Study

In a first part, we investigate purely thin mechanical structures, and we compare our results with those of the Mindlin–Reissner plate bending element of Hughes and Tezduyar [7] (referred to as MR\_HT) and the Mindlin–Reissner plate bending element of Simo and Rifai (referred to as MT\_SR). The latter are based on the method of enhanced assumed strains [11]. Contrary to these two formulations, we perform a full 3D-analysis of the structures with hexahedral elements of 2nd degree. Specifically, we apply our new approach with balanced reduced integration (referred as *present*) as well as standard finite elements that do not contain precautions to locking (referred as *standard*).

The three structures of investigation are a square, a rhombic, and a circular plate. The data are chosen as described in [11]. In these examples, a simply supported boundary condition is used on the lateral boundary. This means in our displacement formulation that we set the mechanical displacement in thickness direction for all nodes along the bottom line of the outer boundary to zero (see e.g. Fig. 1). If a symmetry of the plate is exploit, the computation need only be performed on a half or a quarter of the plate and the displacement in the direction of the normal is set to zero on the 'symmetry boundaries'.

In the second part, we first discuss results of a harmonic analysis for a circular plate in order to test our approach for describing the dynamic behavior of thin mechanical structures. We then investigate in mechanical structures driven by a thin piezoelectric layer.

Finally, we test our approach by computing the sound pressure level generated by a piezoelectric loudspeaker.

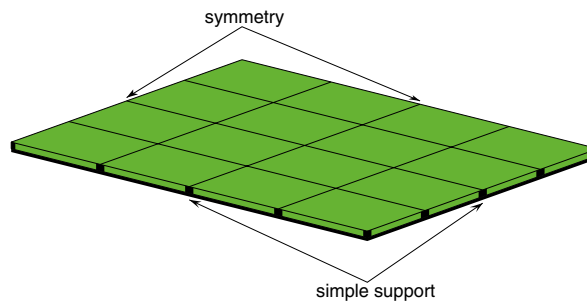


Figure 1. Mesh for rectangular plate (due to symmetry, only one fourth of the structure is meshed)

### 5.1. Square Plate

In a first numerical example, we consider the bending of a square plate. The plate has a length of  $L = 10$  m, a thickness of 0.1 m and is simply supported. The modulus of elasticity  $E$  and Poisson ratio  $\nu$  are chosen to be  $10.92 \text{ N/m}^2$  and 0.3, and the plate is loaded by a uniform pressure  $p$  of  $1 \text{ N/m}^2$ . We use symmetry boundary conditions in order to just model a quadrant. Figure 1 displays the mesh using 4 by 4 elements in the plane and one element in the thickness direction.

Table III shows the numerical results. [A value of  $4.0644 \cdot 10^4$  is reported in [11] for the result of a series.] Moreover the stiffness of the 3D model is 0.5 – 1% smaller than that of the plate.



Table III. Bending of a square plate (all meshes just have one finite element in thickness direction)

mesh	center displacement $\times 10^4$			
	MR_HT	MT_SR	standard	present
2 x 2	3.9712	3.9712	3.6688	4.0036
4 x 4	4.0439	4.0436	4.0438	4.1766
8 x 8	4.0593	4.0593	4.0711	4.1497
16 x 16	4.0632	4.0632	4.0831	4.1173
32 x 32			4.0913	4.1035
64 x 64			4.0947	4.1025

This is explained by the additional degrees of freedom of the 3D model. It is not an effect of the reduced integration since the standard finite elements show the same effect asymptotically.

### 5.2. Rhombic Plate

The  $30^\circ$  skew plate, as displayed in Fig. 2, has a side length of 100 m, thickness of 1 m and is loaded by a uniform pressure of  $1\text{ N/m}^2$ . The modulus of elasticity  $E$  is chosen to be  $10^3\text{ N/m}^2$  and the Poisson ratio  $\nu$  to 0.3. All along the boundary the plate is simple supported,

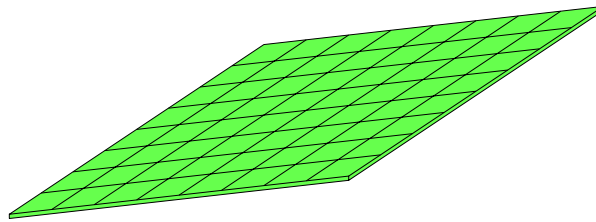


Figure 2. Mesh for rhombic plate

which means for a displacement formulation setting the mechanical displacement in thickness direction to zero. The results of our computations as well as the one reported in [11] are listed in Tab. IV.

There is the well-known complication that we have not only the danger of locking, but also less regularity at the  $120^\circ$  corner. Therefore, the convergence of the 3D finite element computations is slower. [Note that the FE results of the plate models do not reflect the reported result of a series which is  $4.455 \cdot 10^{-2}$ .]

### 5.3. Circular Plate

For the circular plate example we use the same material parameters as for the square plate above. The radius is chosen to be 5 m, the thickness 0.1 m, and the plate is loaded by a uniform pressure of  $1\text{ N/m}^2$ . The plate is simply supported on its boundary. Again, we model just one quadrant of the plate for symmetry reasons. The thickness of the plate will be discretized for the computation by one element, and we will use isoparametric elements in the plane as

Table IV. Bending of a rhombic plate (all meshes just have one finite element in thickness direction)

mesh	center displacement $\times 10^{-2}$			
	MR_HT	MT_SR	standard	present
4 x 4	3.8803	3.9841	1.9628	3.0288
8 x 8	4.1565	4.2727	3.0536	3.8631
16 x 16	4.3883	4.4668	3.8283	4.3217
32 x 32			4.3270	4.5258
64 x 64			4.5474	4.6593
128 x 128			4.6460	4.6965

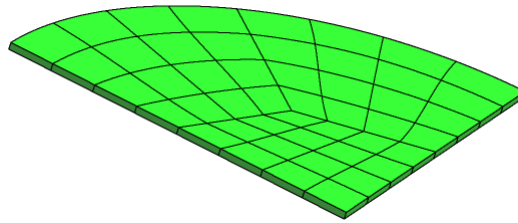


Figure 3. Mesh for circular plate

shown in Fig. 3. Since isoparametric elements of second degree are used, the curved boundary is approximated by quadratic polynomials. – Table V contains the numerical results.

Table V. Bending of a circular plate (all meshes just have one finite element in thickness direction)

mesh	center displacement $\times 10^4$			
	MR_HT	MT_SR	standard	present
12 elements	3.9070	3.6966	3.7595	3.8788
48 elements	3.9649	3.9140	3.8366	3.8784
192 elements	3.9789	3.9664	3.8640	3.8741
768 elements	3.9822	3.9791	3.8696	3.8726

#### 5.4. Dynamic Behavior of a Circular Plate

For many applications, the dynamic behavior of thin mechanical structures is of great interest. For this reason, we perform a harmonic analysis over a certain frequency range, and we will compare the standard formulation with our new approach. We set the radius of the plate to 20 mm, its thickness to 0.2 mm. The modulus of elasticity  $E$  is chosen to be  $4 \cdot 10^{10}$  N/m<sup>2</sup>, the Poisson ratio  $\nu = 0.3$ , and the density  $\rho = 8.410^3$  kg/m<sup>3</sup>. The two damping parameters  $\alpha_M$  (proportional to the mass) and  $\alpha_K$  (proportional to the stiffness) have been chosen as  $6.2675$  and  $3.39789 \cdot 10^{-7}$ , resp., constant over the frequency range of interest.

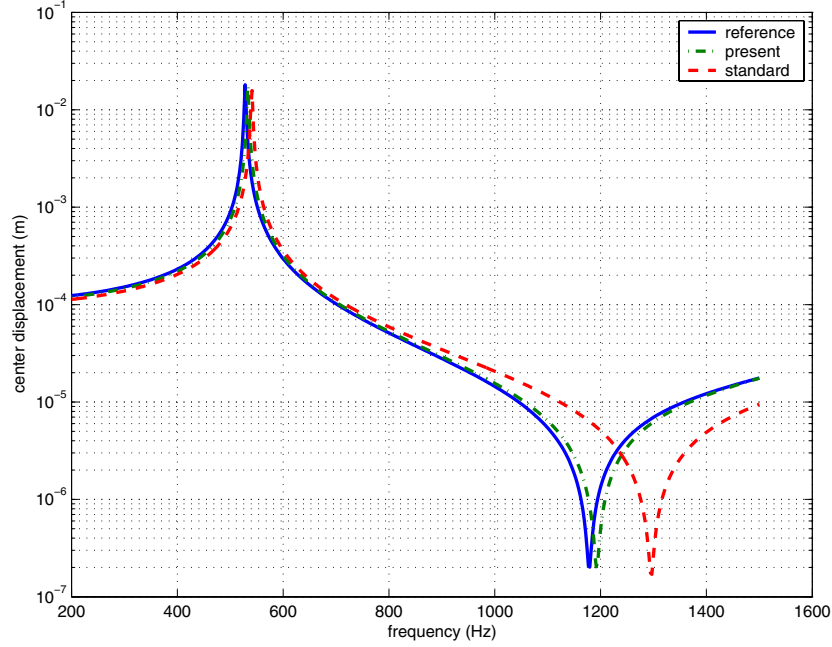


Figure 4. Amplitude of center displacement over frequency

The results of the standard and the present approach are shown in Fig. 4 for the coarsest mesh with 12 elements; (see Sec. 5.3). For comparison we have also computed the center displacement over the frequency range on the finest mesh with 768 elements, referred to as *reference* in Fig. 4. As can be seen, our new formulation captures the center displacement even on the coarse mesh quite well, whereas the standard formulation shows quite large differences at higher frequencies.

##### 5.5. Rectangular Plate with Piezoelectric Layer

We now consider a rectangular plate of thickness 0.1 mm covered by a piezoelectric layer of the same thickness. The side lengths are 40 mm and 20 mm and the structure is simply supported. We use a fixed discretization of one element for both the plate as well as the piezoelectric layer in thickness direction and vary the in-plane discretization as shown in Fig. 5. The material parameters for the plate are chosen to be  $E = 7.08 \cdot 10^{10}$ ,  $\nu = 0.338$  and  $\rho = 2.7 \cdot 10^3 \text{ N/m}^2$ . The piezoelectric layer is made of PZT-5H with  $\rho = 7.75 \cdot 10^3 \text{ N/m}^2$  and the following material tensors:

$$[\mathbf{c}^E] = \begin{pmatrix} 1.26 \cdot 10^{11} & 7.95 \cdot 10^{10} & 8.41 \cdot 10^{10} & 0.0 & 0.0 & 0.0 \\ 7.95 \cdot 10^{10} & 1.26 \cdot 10^{11} & 8.41 \cdot 10^{10} & 0.0 & 0.0 & 0.0 \\ 8.41 \cdot 10^{10} & 8.41 \cdot 10^{10} & 1.17 \cdot 10^{11} & 0.0 & 0.0 & 0.0 \\ 0.0 & 0.0 & 0.0 & 2.3 \cdot 10^{10} & 0.0 & 0.0 \\ 0.0 & 0.0 & 0.0 & 0.0 & 2.3 \cdot 10^{10} & 0.0 \\ 0.0 & 0.0 & 0.0 & 0.0 & 0.0 & 2.32 \cdot 10^{10} \end{pmatrix}$$

$$[e] = \begin{pmatrix} 0.0 & 0.0 & 0.0 & 0.0 & 17.0 & 0.0 \\ 0.0 & 0.0 & 0.0 & 17.0 & 0.0 & 0.0 \\ -6.5 & -6.5 & 23.3 & 0.0 & 0.0 & 0.0 \end{pmatrix}$$

$$[\epsilon^S] = \begin{pmatrix} 1.51 \cdot 10^{-8} & 0.0 & 0.0 \\ 0.0 & 1.51 \cdot 10^{-8} & 0.0 \\ 0.0 & 0.0 & 1.27 \cdot 10^{-8} \end{pmatrix}$$

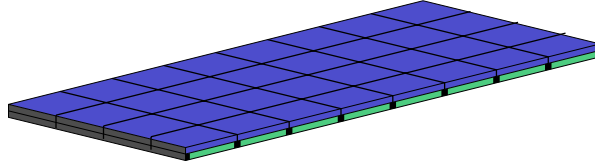


Figure 5. Mesh for mechanical structure with piezoelectric layer

In Tab. VI we list the results obtained by standard FE-formulation using 2nd order finite elements and our approach as a function of the ratio  $h/t$ , where  $h$  denotes the discretization in the plate plane and  $t$  the thickness of the rectangular plate and piezoelectric layer, respectively. Therewith, we obtain with this value the maximal ratio of the side length of the finite elements.

Table VI. Bending of rectangular mechanical structure with piezoelectric layer

	center displacement $\times 10^{-6}$			
	$h/t = 50$	$h/t = 25$	$h/t = 10$	$h/t = 5$
standard	11.290	11.580	11.669	11.652
present	11.398	11.764	11.805	11.721

### 5.6. Practical example

Figure 6 displays the grid of a configuration that is used for piezoelectric loudspeakers. A thin plate is coated by 80% with a thin piezoelectric layer. The dimensions of the plate are 30 mm by 40 mm with a thickness of  $250 \mu\text{m}$ , and the thickness of the piezoelectric layer is  $50 \mu\text{m}$ . The main goal for the numerical computation is to optimize the geometry as well as material parameter towards an acoustic pressure response, which should be as flat as possible over a wide frequency range by simultaneously being as large as possible. Therewith, the task is a fast and reliable (forward) computation of this pressure response over the frequency range of interest. A first approximation of the sound pressure response is the deformed volume  $V_{\text{def}}^2$  of the plate

$$p_{\text{acoustic}} \approx \text{const.} \cdot f^2 V_{\text{def}}^2 \quad (25)$$

where  $f$  is the frequency. The calculations are performed with the same material parameters as in Sec. 5.4.

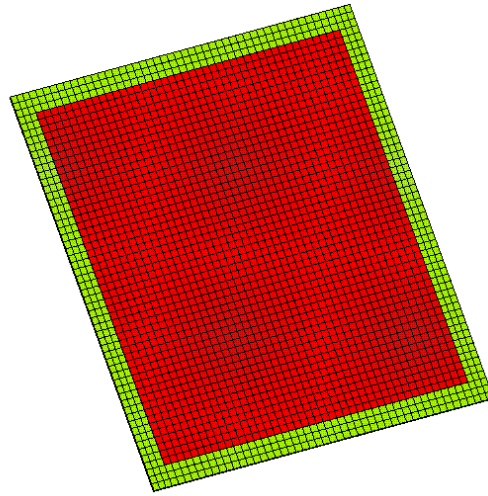


Figure 6. Setup of the piezoelectric loudspeaker and coarse mesh

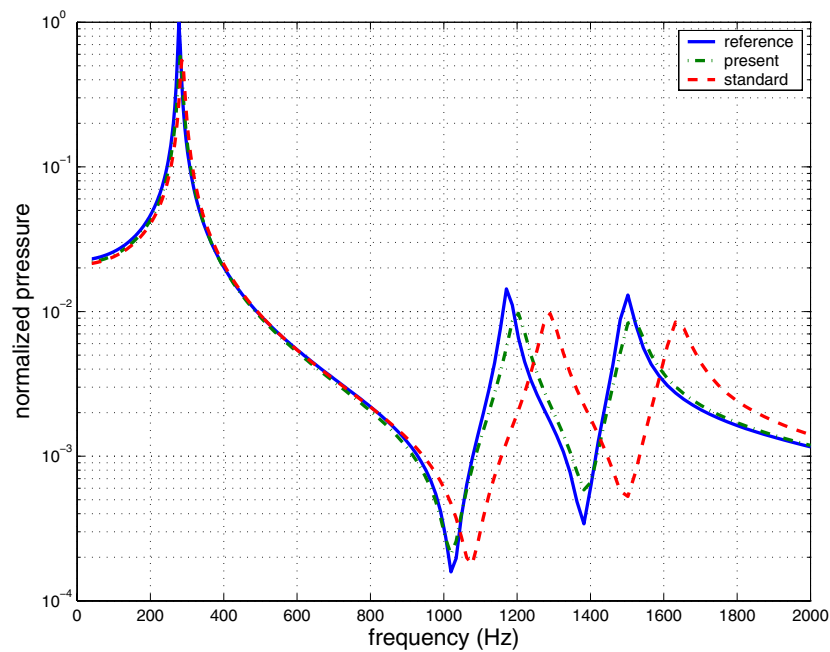


Figure 7. Normalized pressure over frequency range

In a first step, we have computed a *reference solution* by a very fine discretization exhibiting 4136 3D hexahedral 2nd order finite elements and resulting in 71219 unknowns. In a second step we have then coarsened the mesh up to 202 3D hexahedral 2nd order finite elements

resulting in 3891 unknowns. Figure 7 shows the reference solution on the fine grid and the computed solutions with the standard formulation as well as the present formulation on the coarse mesh. Very similar to Sec. 5.4 our new formulation obviously resolves the dynamic behavior already on a quite coarse grid very well.

## 6. Conclusion

We have considered plates on which piezoelectric material is mounted. Since such a compound structure builds a thin-walled body, the displacement formulation without extra design would suffer from locking. An efficient selected reduced integration method for 3D finite elements has been derived from recent results on Mindlin–Reissner plates.

The implementation is less involved than the popular EAS method. Numerical examples for static and time-dependent problems are presented, which show very satisfactory results.

### *Acknowledgment*

The main part of this work was done during the stay of the authors at RICAM, Linz, Austria. The authors are grateful to Professor Ulrich Langer for the stimulating atmosphere at the "Special Radon Semester on Computational Mechanics" that he organized in Linz in 2005.

## REFERENCES

1. D.N. Arnold and F. Brezzi. Some new elements for the Reissner–Mindlin plate model. In *Boundary Value Problems for Partial Differential Equations and Applications* (J.-L. Lions and C. Baiocchi, eds.) pp. 287–292, Masson, Paris, 1993.
2. D.N. Arnold and R.S. Falk. A uniformly accurate finite element method for the Mindlin–Reissner plate. *SIAM J. Numer. Anal.* 26, 1276–1290, 1989.
3. T. Belytschko, K. Lui, W, and B. Moran. *Nonlinear Finite Elements for Continua and Structures*. Wiley, 2000.
4. D. Braess. *Finite Elements: Theory, Fast Solvers, and Applications in Elasticity Theory*, Cambridge University Press, 2001.
5. D. Chapelle and R. Stenberg. An optimal low-order locking-free finite element method for Mindlin–Reissner plates. *Math. Models and Methods in Appl. Sci.* 8, 407–430, 1998.
6. T. Hughes. *The Finite Element Method*. Prentice-Hall, New Jersey, 1 edition, 1987.
7. T. Hughes and T. Tezduyar. Finite elements based upon Mindlin plate theory with particular reference to the four-node bilinear isoparametric element. *J. Appl. Mech., ASME*, pages 587–596b, 1981.
8. M. Kaltenbacher. *Numerical Simulation of Mechatronic Sensors and Actuators*. Springer Berlin-Heidelberg-New York, 2004. ISBN: 3-540-20458-X.
9. J. Pitkäranta and M. Suri. Upper and lower error bounds for plate-bending finite elements. *Numer. Math.*, 84, 611–648, (2000)
10. S. Reese. A large deformation solid-shell concept based on reduced integration with hourglass instability. *Int. J. Numer. Methods Eng.*, (in press)
11. J. Simo and M. Rifai. A class of mixed assumed strain methods and the method of incompatible modes. *Int. J. Numer. Methods Eng.*, 29:1595–1638, 1990.
12. M. Vogelius and I. Babuška. On a dimensional reduction method. I: The optimal selection of basis functions. *Math. Comput.*, 37, 31–46 (1981)